

LISA Data Analysis using MCMC methods

Neil J. Cornish and Jeff Crowder

Department of Physics, Montana State University, Bozeman, MT 59717

The Laser Interferometer Space Antenna (LISA) is expected to simultaneously detect many thousands of low frequency gravitational wave signals. This presents a data analysis challenge that is very different to the one encountered in ground based gravitational wave astronomy. LISA data analysis requires the identification of individual signals from a data stream containing an unknown number of overlapping signals. Because of the signal overlaps, a global fit to all the signals has to be performed in order to avoid biasing the solution. However, performing such a global fit requires the exploration of an enormous parameter space with a dimension upwards of 50,000. Markov Chain Monte Carlo (MCMC) methods offer a very promising solution to the LISA data analysis problem. MCMC algorithms are able to efficiently explore large parameter spaces, simultaneously providing parameter estimates, error analysis, and even model selection. Here we present the first application of MCMC methods to simulated LISA data and demonstrate the great potential of the MCMC approach. Our implementation uses a generalized F-statistic to evaluate the likelihoods, and simulated annealing to speed convergence of the Markov chains. As a final step we super-cool the chains to extract maximum likelihood estimates, and estimates of the Bayes factors for competing models. We find that the MCMC approach is able to correctly identify the number of signals present, extract the source parameters, and return error estimates consistent with Fisher information matrix predictions.

I. INTRODUCTION

The LISA observatory [1] has incredible science potential, but that potential can only be fully realized by employing advanced data analysis techniques. LISA will explore the low frequency portion of the gravitational wave spectrum, which is thought to be home to a vast number of sources. Since gravitational wave sources typically evolve on timescales that are long compared to the gravitational wave period, individual low frequency sources will be “on” for large fractions of the nominal three year LISA mission lifetime. Moreover, unlike a traditional telescope, LISA can not be pointed at a particular point on the sky. The upshot is that the LISA data stream will contain the signals from tens of thousands of individual sources, and ways must be found to isolate individual voices from the crowd. This “Cocktail Party Problem” is the central issue in LISA data analysis.

The types of sources LISA is expected to detect include galactic and extra-galactic compact stellar binaries, super massive black hole binaries, and extreme mass ratio inspirals of compact stars into supermassive black holes (EMRIs). Other potential sources include intermediate mass black hole binaries, cosmic strings, and a cosmic gravitational wave background produced by processes in the early universe. In the case of compact stellar binaries [2, 3, 4, 5, 6] and EMRIs [7, 8], the number of sources is likely to be so large that it will be impossible to resolve all the sources individually, so that there will be a residual signal that is variously referred to as a confusion limited background or confusion noise. It is important that this confusion noise be made as small as possible so as not to hinder the detection of other high value targets. Several estimates of the confusion noise level have been made [4, 5, 6, 9, 10, 11], and they all suggest that unresolved signals will be the dominant

source of low frequency noise for LISA. However, these estimates are based on assumptions about the efficacy of the data analysis algorithms that will be used to identify and regress sources from the LISA data stream, and it is unclear at present how reasonable these assumptions might be. Indeed, the very notion that one can first clean the data stream of one type of signal before moving on to search for other targets is suspect as the gravitational wave signals from different sources are not orthogonal. For example, when the signal from a supermassive black hole binary sweeps past the signal from a white dwarf binary of period T , the two signals will have significant overlap for a time interval equal to the geometric mean of T and t_c , where t_c is the time remaining before the black holes merge. Thus, by a process dubbed “the white dwarf transform,” it is possible to decompose the signal from a supermassive black hole binary into signals from a collection of white dwarf binaries.

As described in §II, optimal filtering of the LISA data would require the construction of a filter bank that described the signals from every source that contributes to the data stream. In principle one could construct a vast template bank describing all possible sources and look for the best match with the data. In practice the enormous size of the search space and the presence of unmodeled sources renders this direct approach impractical. Possible alternatives to a full template based search include iterative refinement of a source-by-source search, ergodic exploration of the parameter space using Markov Chain Monte Carlo (MCMC) algorithms, Darwinian optimization by genetic algorithms, and global iterative refinement using the Maximum Entropy Method (MEM). Each approach has its strengths and weakness, and at this stage it is not obvious which approach will prove superior.

Here we apply the popular Markov Chain Monte

Carlo [12, 13] method to simulated LISA data. This is not the first time that MCMC methods have been applied to gravitational wave data analysis, but it is first outing with realistic simulated LISA data. Our simulated data streams contain the signals from multiple galactic binaries. Previously, MCMC methods have been used to study the extraction of coalescing binary [14] and spinning neutron star [15] signals from terrestrial interferometers. More recently, MCMC methods have been applied to a simplified toy problem [16] that shares some of the features of the LISA cocktail party problem. These studies have shown that MCMC methods hold considerable promise for gravitational wave data analysis, and offer many advantages over the standard template grid searches. For example, the EMRI data analysis problem [7, 8] is often cited as the greatest challenge facing LISA science. Neglecting the spin of the smaller body yields a 14 dimensional parameter space, which would require $\sim 10^{40}$ templates to explore in a grid based search [8]. This huge computational cost arises because grid based searches scale geometrically with the parameter space dimension D . In contrast, the computational cost of MCMC based searches scale linearly with the D . In fields such as finance, MCMC methods are routinely applied to problems with $D > 1000$, making the LISA EMRI problem seem trivial in comparison. A *Google* search on “Markov Chain Monte Carlo” returns almost 250,000 results, and a quick scan of these pages demonstrates the wide range of fields where MCMC methods are routinely used. We found it amusing that one of the *Google* search results is a link to the *PageRank* [17] MCMC algorithm that powers the *Google* search engine.

The structure of the paper follows the development sequence we took to arrive at a fast and robust MCMC algorithm. In §II we outline the LISA data analysis problem and the particular challenges posed by the galactic background. A basic MCMC algorithm is introduced in §III and applied to a full 7 parameter search for a single galactic binary. A generalized multi-channel, multi-source F-statistic for reducing the search space from $D = 7N$ to $D = 3N$ is described in §IV. The performance of a basic MCMC algorithm that uses the F-statistic is studied in §V and a number of problems with this simple approach are identified. A more advanced mixed MCMC algorithm that incorporates simulated annealing is introduced in §VI and is successfully applied to multi-source searches. The issue of model selection is addressed in §VII, and approximate Bayes factor are calculated by super-cooling the Markov Chains to extract maximum likelihood estimates. We conclude with a discussion of future refinements and extensions of our approach in §VIII.

II. THE COCKTAIL PARTY PROBLEM

Space based detectors such as LISA are able to return several interferometer outputs [18]. The strains

registered in the interferometer in response to a gravitational wave pick up modulations due to the motion of the detector. The orbital motion introduces amplitude, frequency, and phase modulation into the observed gravitational wave signal. The amplitude modulation results from the detector’s antenna pattern being swept across the sky, the frequency modulation is due to the Doppler shift from the relative motion of the detector and source, and the phase modulation results from the detector’s varying response to the two gravitational wave polarizations [19, 20]. These modulations encode information about the location of the source. The modulations spread a monochromatic signal over a bandwidth $\Delta f \sim (9 + 6(f/\text{mHz}) \sin \theta) f_m$, where θ is the co-latitude of the source and $f_m = 1/\text{year}$ is the modulation frequency. In the low frequency limit, where the wavelengths are large compared to the armlengths of the detector, the interferometer outputs $s_\alpha(t)$ can be combined to simulate the response of two independent 90 degree interferometers, $s_I(t)$ and $s_{II}(t)$, rotated by 45 degrees with respect to each other [19, 21]. This allows LISA to measure both polarizations of the gravitational wave simultaneously. A third combination of signals in the low frequency limit yields the symmetric Sagnac variable [18], which is insensitive to gravitational waves and can be used to monitor the instrument noise. When the wavelengths of the gravitational waves become comparable to the size of the detector, which for LISA corresponds to frequencies above 10 mHz, the interferometry signals can be combined to give three independent time series with comparable sensitivities [21].

The output of each LISA data stream can be written as

$$s_\alpha(t) = h_\alpha(t, \vec{\lambda}) + n_\alpha(t) = \sum_{i=1}^N h_\alpha^i(t, \vec{\lambda}_i) + n_\alpha(t). \quad (1)$$

Here $h_\alpha^i(t, \vec{\lambda}_i)$ describes the response registered in detector channel α to a source with parameters $\vec{\lambda}_i$. The quantity $h_\alpha(t, \vec{\lambda})$ denotes the combined response to a collection of N sources with total parameter vector $\vec{\lambda} = \sum_i \vec{\lambda}_i$ and $n_\alpha(t)$ denotes the instrument noise in channel α . Extracting the parameters of each individual source from the combined response to all sources defines the LISA cocktail party problem. In practice it will be impossible to resolve all of the millions of signals that contribute to the LISA data streams. For one, there will not be enough bits of information in the entire LISA data archive to describe all N sources in the Universe with signals that fall within the LISA band. Moreover, most sources will produce signals that are well below the instrument noise level, and even after optimal filtering most of these sources will have signal to noise ratios below one. A more reasonable goal might be to provide estimates for the parameters describing each of the N' sources that have integrated signal to noise ratios (SNR) above some threshold (such as $\text{SNR} > 5$), where it is now understood that the noise includes the instrument noise,

residuals from the regression of bright sources, and the signals from unresolved sources.

While the noise will be neither stationary nor Gaussian, it is not unreasonable to hope that the departures from Gaussianity and stationarity will be mild. It is well known that matched filtering is the optimal linear signal processing technique for signals with stationary Gaussian noise [22, 23]. Matched filtering is used extensively in all fields of science, and is a popular data analysis technique in ground based gravitational wave astronomy [24, 25, 26, 27, 28, 29, 30, 31, 32, 33, 34, 35]. Switching to the Fourier domain, the signal can be written as $\tilde{s}_\alpha(f) = \tilde{h}_\alpha(f, \vec{\lambda}') + \tilde{n}_\alpha(f)$, where $\tilde{n}_\alpha(f)$ includes instrument noise and confusion noise, and the signals are described by parameters $\vec{\lambda}'$. Using the standard noise weighted inner product for the independent data channels over a finite observation time T ,

$$(a|b) = \frac{2}{T} \sum_\alpha \sum_f \frac{\tilde{a}_\alpha^*(f) \tilde{b}_\alpha(f) + \tilde{a}_\alpha(f) \tilde{b}_\alpha^*(f)}{S_n^\alpha(f)}, \quad (2)$$

a Wiener filter statistic can be defined:

$$\rho(\vec{\lambda}) = \frac{(s|h(\vec{\lambda}))}{\sqrt{(h(\vec{\lambda})|h(\vec{\lambda}))}}. \quad (3)$$

The noise spectral density $S_n(f)$ is given in terms of the autocorrelation of the noise

$$\langle n(f)n^*(f') \rangle = \frac{T}{2} \delta_{ff'} S_n(f). \quad (4)$$

Here and elsewhere angle brackets $\langle \rangle$ denote an expectation value. An estimate for the source parameters $\vec{\lambda}'$ can be found by maximizing $\rho(\vec{\lambda})$. If the noise is Gaussian and a signal is present, $\rho(\vec{\lambda})$ will be Gaussian distributed with unit variance and mean equal to the integrated signal to noise ratio

$$\text{SNR} = \langle \rho(\vec{\lambda}') \rangle = \sqrt{(h(\vec{\lambda}')|h(\vec{\lambda}'))}. \quad (5)$$

The optimal filter for the LISA signal (1) is a matched template describing all N' resolvable sources. The number of parameters d_i required to describe a source ranges from 7 for a slowly evolving circular galactic binary to 17 for a massive black hole binary. A reasonable estimate [10] for N' is around 10^4 , so the full parameter space has dimension $D = \sum_i d_i \sim 10^5$. Since the number of templates required to uniformly cover a parameter space grows exponentially with D , a grid based search using the full optimal filter is out of the question. Clearly an alternative approach has to be found. Moreover, the number of resolvable sources N' is not known a priori, so some stopping criteria must be found to avoid over-fitting the data.

Existing approaches to the LISA cocktail party problem employ iterative schemes. The first such approach was dubbed “gCLEAN” [41] due to its similarity with

the “CLEAN” [42] algorithm that is used for astronomical image reconstruction. The “gCLEAN” procedure identifies and records the brightest source that remains in the data stream, then subtracts a small amount of this source. The procedure is iterated until a prescribed residual is reached, at which time the individual sources are reconstructed from the subtraction record. A much faster iterative approach dubbed “Slice & Dice” [43] was recently proposed that proceeds by identifying and fully subtracting the brightest source that remains in the data stream. A global least squares re-fit to all the current list of sources is then performed, and the new parameter record is used to produce a regressed data stream for the next iteration. Bayes factors are used to provide a stopping criteria.

There is always the danger with iterative approaches that the procedure “gets off on the wrong foot,” and is unable to find its way back to the optimal solution. This can happen when two signals have a high degree of overlap. A very different approach to the LISA source confusion problem is to solve for all sources simultaneously using ergodic sampling techniques. Markov Chain Monte Carlo (MCMC) [45, 46] is a method for estimating the posterior distribution, $p(\vec{\lambda}|s)$, that can be used with very large parameter spaces. The method is now in widespread use in many fields, and is starting to be used by astronomers and cosmologists. One of the advantages of MCMC is that it combines detection, parameter estimation, and the calculation of confidence intervals in one procedure, as everything one can ask about a model is contained in $p(\vec{\lambda}|s)$. Another nice feature of MCMC is that there are implementations that allow the number of parameters in the model to be variable, with built in penalties for using too many parameters in the fit. In an MCMC approach, parameter estimates from Wiener matched filtering are replaced by the Bayes estimator [39]

$$\lambda_B^i(s) = \int \lambda^i p(\vec{\lambda}|s) d\vec{\lambda}, \quad (6)$$

which requires knowledge of $p(\vec{\lambda}|s)$ - the posterior distribution of $\vec{\lambda}$ (*i.e.* the distribution of $\vec{\lambda}$ conditioned on the data s). By Bayes theorem, the posterior distribution is related to the prior distribution $p(\vec{\lambda})$ and the likelihood $p(s|\vec{\lambda})$ by

$$p(\vec{\lambda}|s) = \frac{p(\vec{\lambda})p(s|\vec{\lambda})}{\int p(\vec{\lambda}')p(s|\vec{\lambda}')d\vec{\lambda}'}. \quad (7)$$

Until recently the Bayes estimator was little used in practical applications as the integrals appearing in (6) and (7) are often analytically intractable. The traditional solution has been to use approximations to the Bayes estimator, such as the maximum likelihood estimator described below, however advances in the Markov Chain Monte Carlo technique allow direct numerical estimates to be made.

When the noise $n(t)$ is a normal process with zero mean, the likelihood is given by [36]

$$p(s|\vec{\lambda}) = C \exp \left[-\frac{1}{2} \left((s - h(\vec{\lambda})) | (s - h(\vec{\lambda})) \right) \right], \quad (8)$$

where the normalization constant C is independent of s . In the large SNR limit the Bayes estimator can be approximated by finding the dominant mode of the posterior distribution, $p(\vec{\lambda}|s)$, which Finn [36] and Cutler & Flanagan[28] refer to as a maximum likelihood estimator. Other authors [37, 38] define the maximum likelihood estimator to be the value of $\vec{\lambda}$ that maximizes the likelihood, $p(s|\vec{\lambda})$. The former has the advantage of incorporating prior information, but the disadvantage of not being invariant under parameter space coordinate transformations. The latter definition corresponds to the standard definition used by most statisticians, and while it does not take into account prior information, it is coordinate invariant. The two definitions give the same result for uniform priors, and very similar results in most cases (the exception being where the priors have a large gradient at maximum likelihood).

The standard definition of the likelihood yields an estimator that is identical to Wiener matched filtering[40]. Absorbing normalization factors by adopting the inverted relative likelihood $\mathcal{L}(\vec{\lambda}) = p(s|0)/p(s|\vec{\lambda})$, we have

$$\log \mathcal{L}(\vec{\lambda}) = (s|h(\vec{\lambda})) - \frac{1}{2}(h(\vec{\lambda})|h(\vec{\lambda})). \quad (9)$$

In the gravitational wave literature the quantity $\log \mathcal{L}(\vec{\lambda})$ is usually referred to as the log likelihood, despite the inversion and rescaling. Note that

$$\langle \log \mathcal{L}(\vec{\lambda}') \rangle = \frac{1}{2} \langle \rho(\vec{\lambda}') \rangle^2 = \frac{1}{2} \text{SNR}^2. \quad (10)$$

The maximum likelihood estimator (MLE), $\vec{\lambda}_{\text{ML}}$, is found by solving the coupled set of equations $\partial \log \mathcal{L} / \partial \lambda^i = 0$. Parameter uncertainties can be estimated from the negative Hessian of $\log \mathcal{L}$, which yields the Fisher Information Matrix

$$\Gamma_{ij}(\vec{\lambda}) = - \left\langle \frac{\partial^2 \log \mathcal{L}(\vec{\lambda})}{\partial \lambda^i \partial \lambda^j} \right\rangle = (h_{,i} | h_{,j}). \quad (11)$$

In the large SNR limit the MLE can be found by writing $\vec{\lambda} = \vec{\lambda}' + \Delta \vec{\lambda}$ and Taylor expanding (9). Setting $\partial \log \mathcal{L} / \partial \Delta \lambda^i = 0$ yields the lowest order solution

$$\lambda_{\text{ML}}^i = \lambda'^i + \Delta \lambda^i = \lambda'^i + \Gamma^{ij}(\vec{\lambda}') (n | h_{,j}). \quad (12)$$

The expectation value of the maximum of the log likelihood is then

$$\langle \log \mathcal{L}(\vec{\lambda}_{\text{ML}}) \rangle = \frac{\text{SNR}^2 + D}{2}. \quad (13)$$

This value exceeds that found in (10) by an amount that depends on the total number of parameters used in the

fit, D , reflecting the fact that models with more parameters generally give better fits to the data. Deciding how many parameters to allow in the fit is an important issue in LISA data analysis as the number of resolvable sources is not known a priori. This issue does not usually arise for ground based gravitational wave detectors as most high frequency gravitational wave sources are transient. The relevant question there is whether or not a gravitational wave signal is present in a section of the data stream, and this question can be dealt with by the Neyman-Pearson test or other similar tests that use thresholds on the likelihood \mathcal{L} that are related to the false alarm and false dismissal rates. Demanding that $\mathcal{L} > 1$ - so it is more likely that a signal is present than not - and setting a detection threshold of $\rho = 5$ yields a false alarm probability of 0.006 and a detection probability of 0.994 (if the noise is stationary and Gaussian). A simple acceptance threshold of $\rho = 5$ for each individual signal used to fit the LISA data would help restrict the total number of parameters in the fit, however there are better criteria that can be employed. The simplest is related to the Neyman-Pearson test and compares the likelihoods of models with different numbers of parameters. For nested models this ratio has an approximately chi squared distribution which allows the significance of adding extra parameters to be determined from standard statistical tables. A better approach is to compute the Bayes factor,

$$B_{XY} = \frac{p_X(s)}{p_Y(s)}, \quad (14)$$

which gives the relative weight of evidence for models X and Y in terms of the ratio of marginal likelihoods

$$p_X(s) = \int p(s|\vec{\lambda}, X) p(\vec{\lambda}, X) d\vec{\lambda}. \quad (15)$$

Here $p(s|\vec{\lambda}, X)$ is the likelihood distribution for model X and $p(\vec{\lambda}, X)$ is the prior distribution for model X . The difficulty with this approach is that the integral in (15) is hard to calculate, though estimates can be made using the Laplace approximation or the Bayesian Information Criterion (BIC) [44]. The Laplace approximation is based on the method of steepest descents, and for uniform priors yields

$$p_X(s) \simeq p(s|\vec{\lambda}_{\text{ML}}, X) \left(\frac{\Delta V_X}{V_X} \right), \quad (16)$$

where $p(s|\vec{\lambda}_{\text{ML}}, X)$ is the maximum likelihood for the model, V_X is the volume of the model's parameter space, and ΔV_X is the volume of the uncertainty ellipsoid (estimated using the Fisher matrix). Models with more parameters generally provide a better fit to the data and a higher maximum likelihood, but they get penalized by the $\Delta V_X / V_X$ term which acts as a built in Occam's razor.

III. MARKOV CHAIN MONTE CARLO

We begin by implementing a basic MCMC search for galactic binaries that searches over the full $D = 7N$ dimensional parameter space using the Metropolis-Hastings [13] algorithm. The idea is to generate a set of samples, $\{\vec{x}\}$, that correspond to draws from the posterior distribution, $p(\vec{\lambda}|s)$. To do this we start at a randomly chosen point \vec{x} and generate a Markov chain according to the following algorithm: Using a proposal distribution $q(\cdot|\vec{x})$, draw a new point \vec{y} . Evaluate the Hastings ratio

$$H = \frac{p(\vec{y})p(s|\vec{y})q(\vec{x}|\vec{y})}{p(\vec{x})p(s|\vec{x})q(\vec{y}|\vec{x})}. \quad (17)$$

Accept the candidate point \vec{y} with probability $\alpha = \min(1, H)$, otherwise remain at the current state \vec{x} (Metropolis rejection [12]). Remarkably, this sampling scheme produces a Markov chain with a stationary distribution equal to the posterior distribution of interest, $p(\vec{\lambda}|s)$, regardless of the choice of proposal distribution [45]. A concise introduction to MCMC methods can be found in the review paper by Andrieu *et al* [47].

On the other hand, a poor choice of the proposal distribution will result in the algorithm taking a very long time to converge to the stationary distribution (known as the burn-in time). Elements of the Markov chain produced during the burn-in phase have to be discarded as they do not represent the stationary distribution. When dealing with large parameter spaces the burn-in time can be very long if poor techniques are used. For example, the Metropolis sampler, which uses symmetric proposal distributions, explores the parameter space with an efficiency of at most $\sim 0.3/D$, making it a poor choice for high dimension searches. Regardless of the sampling scheme, the mixing of the Markov chain can be inhibited by the presence of strongly correlated parameters. Correlated parameters can be dealt with by making a local coordinate transformation at \vec{x} to a new set of coordinates that diagonalises the Fisher matrix, $\Gamma_{ij}(\vec{x})$.

We tried a number of proposal distributions and update schemes to search for a single galactic binary. The results were very disappointing. Bold proposals that attempted large jumps had a very poor acceptance rate, while timid proposals that attempted small jumps had a good acceptance rate, but they explored the parameter space very slowly, and got stuck at local modes of the posterior. Lorentzian proposal distributions fared the best as their heavy tails and concentrated peaks lead to a mixture of bold and timid jumps, but the burn in times were still very long and the subsequent mixing of the chain was torpid. The MCMC literature is full of similar examples of slow exploration of large parameter spaces, and a host of schemes have been suggested to speed up the burn-in. Many of the accelerated algorithms use adaptation to tune the proposal distribution. This violates the Markov nature of the chain as the updates depend on the history of the chain. More complicated adaptive algorithms

have been invented that restore the Markov property by using additional Metropolis rejection steps. The popular Delayed Rejection Method [48] and Reversible Jump Method [49] are examples of adaptive MCMC algorithms. A simpler approach is to use a non-Markov scheme during burn-in, such as adaptation or simulated annealing, then transition to a Markov scheme after burn-in. Since the burn-in portion of the chain is discarded, it does not matter if the MCMC rules are broken (the burn-in phase is more like Las Vegas than Monte Carlo).

Before resorting to complex acceleration schemes we tried a much simpler approach that proved to be very successful. When using the Metropolis-Hastings algorithm there is no reason to restrict the updates to a single proposal distribution. For example, every update could use a different proposal distribution so long as the choice of distribution is not based on the history of the chain. The proposal distributions to be used at each update can be chosen at random, or they can be applied in a fixed sequence. Our experience with single proposal distributions suggested that a scheme that combined a very bold proposal with a very timid proposal would lead to fast burn-in and efficient mixing. For the bold proposal we chose a uniform distribution for each of the source parameters $\vec{\lambda} \rightarrow (A, f, \theta, \phi, \psi, \iota, \varphi_0)$. Here A is the amplitude, f is the gravitational wave frequency, θ and ϕ are the ecliptic co-latitude and longitude, ψ is the polarization angle, ι is the inclination of the orbital plane, and φ_0 is the orbital phase at some fiducial time. The amplitudes were restricted to the range $A \in [10^{-23}, 10^{-21}]$ and the frequencies were restricted to lie within the range of the data snippet $f \in [0.999995, 1.003164]$ mHz (the data snippet contained 100 frequency bins of width $\Delta f = 1/\text{year}$). A better choice would have been to use a cosine distribution for the co-latitude θ and inclination ι , but the choice is not particularly important. When multiple sources were present each source was updated separately during the bold proposal stage. For the timid proposal we used a normal distribution for each eigendirection of the Fisher matrix, $\Gamma_{ij}(\vec{x})$. The standard deviation σ_k for each eigendirection k was set equal to $\sigma_k = 1/\sqrt{\alpha_k D}$, where α_k is the corresponding eigenvalue of $\Gamma_{ij}(\vec{x})$, and $D = 7N$ is the search dimension. The factor of $1/\sqrt{D}$ ensures a healthy acceptance rate as the typical total jump is then $\sim 1\sigma$. All N sources were updated simultaneously during the timid proposal stage. Note that the timid proposal distributions are not symmetric since $\Gamma_{ij}(\vec{x}) \neq \Gamma_{ij}(\vec{y})$. One set of bold proposals (one for each source) was followed by ten timid proposals in a repeating cycle. The ratio of the number of bold to timid proposals impacted the burn-in times and the final mixing rate, but ratios anywhere from 1:1 to 1:100 worked well. We used uniform priors, $p(\vec{x}) = \text{const.}$, for all the parameters, though once again a cosine distribution would have been better for θ and ι . Two independent LISA data channels were simulated directly in the frequency domain using the method described in Ref. [10], with the sources chosen at random using the same uniform distributions employed

TABLE I: 7 parameter MCMC search for a single galactic binary

| | A (10^{-22}) | f (mHz) | θ | ϕ | ψ | ι | φ_0 |
|-------------------------------|--------------------|-----------|----------|--------|--------|---------|-------------|
| $\vec{\lambda}_{\text{True}}$ | 1.73 | 1.0005853 | 0.98 | 4.46 | 2.55 | 1.47 | 0.12 |
| $\vec{\lambda}_{\text{MCMC}}$ | 1.44 | 1.0005837 | 1.07 | 4.42 | 2.56 | 1.52 | 0.15 |
| σ_{Fisher} | 0.14 | 2.2e-06 | 0.085 | 0.051 | 0.054 | 0.050 | 0.22 |
| σ_{MCMC} | 0.14 | 2.4e-06 | 0.089 | 0.055 | 0.058 | 0.052 | 0.23 |

by the bold proposal. The data covers 1 year of observations, and the data snippet contains 100 frequency bins (of width 1/year). The instrument noise was assumed to be stationary and Gaussian, with position noise spectral density $S_n^{\text{pos}} = 4 \times 10^{-22} \text{ m}^2 \text{ Hz}^{-1}$ and acceleration noise spectral density $S_n^{\text{accel}} = 9 \times 10^{-30} \text{ m}^2 \text{ s}^{-4} \text{ Hz}^{-1}$.

Table I summarizes the results of one MCMC run using a model with one source to search for a single source in the data snippet. Burn-in lasted ~ 2000 iterations, and post burn-in the chain was run for 10^6 iterations with a proposal acceptance rate of 77% (the full run took 20 minutes on a Mac G5 2 GHz processor). The chain was used to calculate means and variances for all the parameters. The parameter uncertainty estimates extracted from the MCMC output are compared to the Fisher matrix estimates evaluated at the mean values of the parameters. The source had true SNR = 12.9, and MCMC recovered SNR = 10.7. Histograms of the posterior parameter distributions are shown in Figure 1, where they are compared to the Gaussian approximation to the posterior given by the Fisher matrix. The agreement is impressive, especially considering that the bandwidth of the source is roughly 10 frequency bins, so there are very few noise samples to work with. Similar results were found for other MCMC runs on the same source, and for MCMC runs with other sources. Typical burn-in times were of order 3000 iterations, and the proposal acceptance rate was around 75%.

The algorithm was run successfully on two and three source searches (the model dimension was chosen to match the number of sources in each instance), but on occasions the chain would get stuck at a local mode of the posterior for a large number of iterations. Before attempting to cure this problem with a more refined MCMC algorithm, we decided to eliminate the extrinsic parameters $A, \iota, \psi, \varepsilon_0$ from the search by using a multi-filter generalized F-statistic. This reduces the search dimension to $D = 3N$, with the added benefit that the projection onto the (f, θ, ϕ) sub-space yields a softer target for the MCMC search.

IV. GENERALIZED F-STATISTIC

The F-statistic was originally introduced [38] in the context of ground based searches for gravitational wave signals from rotating Neutron stars. The F-statistic has since been used to search for monochromatic galactic bi-

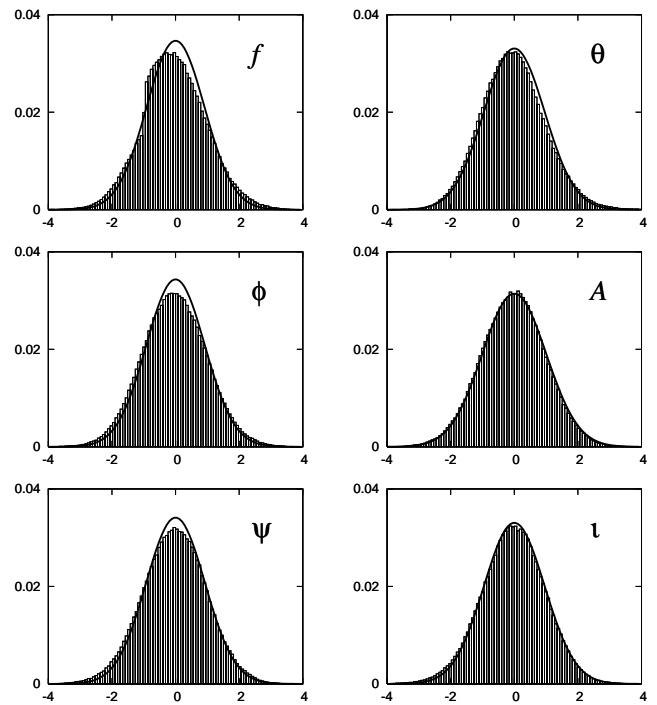


FIG. 1: Histograms showing the posterior distribution (grey) of the parameters. Also shown (black line) is the Gaussian approximation to the posterior distribution based on the Fisher information matrix. The mean values have been subtracted, and the parameters have been scaled by the square root of the variances calculated from the MCMC chains.

aries using simulated LISA data [43, 51]. By using multiple linear filters, the F-statistic is able to automatically extremize the log likelihood over extrinsic parameters, thus reducing the dimension of the search space (the parameter space dimension remains the same).

In the low-frequency limit the LISA response to a gravitational wave with polarization content $h_+(t)$, $h_\times(t)$ can be written as

$$h(t) = h_+(t)F^+(t) + h_\times(t)F^\times(t), \quad (18)$$

where

$$\begin{aligned} F^+(t) &= \frac{1}{2} (\cos 2\psi D^+(t) - \sin 2\psi D^\times(t)) \\ F^\times(t) &= \frac{1}{2} (\sin 2\psi D^+(t) + \cos 2\psi D^\times(t)) \end{aligned} \quad (19)$$

The detector pattern functions $D^+(t)$ and $D^\times(t)$ are given in equations (36) and (37) of Ref.[50]. To leading post-Newtonian order a slowly evolving, circular binary has polarization components

$$\begin{aligned} h_+(t) &= A(1 + \cos^2 \iota) \cos(\Phi(t) + \varphi_0) \\ h_\times(t) &= -2A \cos \iota \sin(\Phi(t) + \varphi_0). \end{aligned} \quad (20)$$

The gravitational wave phase

$$\Phi(t; f, \theta, \phi) = 2\pi f t + 2\pi f A U \sin \theta \cos(2\pi f_m t - \phi), \quad (21)$$

couples the sky location and the frequency through the term that depends on the radius of LISA's orbit, 1 AU, and the orbital modulation frequency, $f_m = 1/\text{year}$. The gravitational wave amplitude, A , is effectively constant for the low frequency galactic sources we are considering. Using these expressions (18) can be written as

$$h(t) = \sum_{i=1}^4 a_i(A, \psi, \iota, \varphi_0) A^i(t; f, \theta, \phi), \quad (22)$$

where the time-independent amplitudes a_i are given by

$$\begin{aligned} a_1 &= \frac{A}{2} ((1 + \cos^2 \iota) \cos \varphi_0 \cos 2\psi - 2 \cos \iota \sin \varphi_0 \sin 2\psi), \\ a_2 &= -\frac{A}{2} (2 \cos \iota \sin \varphi_0 \cos 2\psi + (1 + \cos^2 \iota) \cos \varphi_0 \sin 2\psi), \\ a_3 &= -\frac{A}{2} (2 \cos \iota \cos \varphi_0 \sin 2\psi + (1 + \cos^2 \iota) \sin \varphi_0 \cos 2\psi), \\ a_4 &= \frac{A}{2} ((1 + \cos^2 \iota) \sin \varphi_0 \sin 2\psi - 2 \cos \iota \cos \varphi_0 \cos 2\psi), \end{aligned} \quad (23)$$

and the time-dependent functions $A^i(t)$ are given by

$$\begin{aligned} A^1(t) &= D^+(t; \theta, \phi) \cos \Phi(t; f, \theta, \phi) \\ A^2(t) &= D^\times(t; \theta, \phi) \cos \Phi(t; f, \theta, \phi) \\ A^3(t) &= D^+(t; \theta, \phi) \sin \Phi(t; f, \theta, \phi) \\ A^4(t) &= D^\times(t; \theta, \phi) \sin \Phi(t; f, \theta, \phi). \end{aligned} \quad (24)$$

Defining the four constants $N^i = (s|A^i)$ and using (22) yields a solution for the amplitudes a_i :

$$a_i = (M^{-1})_{ij} N^j, \quad (25)$$

where $M^{ij} = (A^i|A^j)$. The output of the four linear filters, N^i , and the 4×4 matrix M^{ij} can be calculated using the same fast Fourier space techniques [10] used to generate the full waveforms. Substituting (22) and (25) into expression (9) for the log likelihood yields the F-statistic

$$\mathcal{F} = \log \mathcal{L} = \frac{1}{2} (M^{-1})_{ij} N^i N^j. \quad (26)$$

The F-statistic automatically maximizes the log likelihood over the extrinsic parameters A , ι , ψ and φ_0 , and reduces the search to the sub-space spanned by f , θ and ϕ . The extrinsic parameters can be recovered from the a_i 's via

$$\begin{aligned} A &= \frac{A_+ + \sqrt{A_+^2 - A_\times^2}}{2} \\ \psi &= \frac{1}{2} \arctan \left(\frac{A_+ a_4 - A_\times a_1}{-(A_\times a_2 + A_+ a_3)} \right) \\ \iota &= \arccos \left(\frac{-A_\times}{A_+ + \sqrt{A_+^2 - A_\times^2}} \right) \\ \varphi_0 &= \arctan \left(\frac{c(A_+ a_4 - A_\times a_1)}{-c(A_\times a_2 + A_+ a_3)} \right) \end{aligned} \quad (27)$$

where

$$\begin{aligned} A_+ &= \sqrt{(a_1 + a_4)^2 + (a_2 - a_3)^2} \\ &\quad + \sqrt{(a_1 - a_4)^2 + (a_2 + a_3)^2} \\ A_\times &= \sqrt{(a_1 + a_4)^2 + (a_2 - a_3)^2} \\ &\quad - \sqrt{(a_1 - a_4)^2 + (a_2 + a_3)^2} \\ c &= \text{sign}(\sin(2\psi)). \end{aligned} \quad (28)$$

The preceding description of the F-statistic automatically incorporates the two independent LISA channels through the use of the dual-channel noise weighted inner product $(a|b)$. The basic F-statistic can easily be generalized to handle N sources. Writing $i = 4K + l$, where K labels the source and $l = 1 \rightarrow 4$ labels the four filters for each source, the F-statistic (26) keeps the same form as before, but now there are $4N$ linear filters N^i , and M^{ij} is a $4N \times 4N$ dimensional matrix. For slowly evolving galactic binaries, which dominate the confusion problem, the limited bandwidth of each individual signal means that the M^{ij} is band diagonal, and thus easily inverted despite its large size.

Since the search is now over the projected sub-space $\{f_J, \theta_J, \phi_J\}$ of the full parameter space, the full Fisher matrix, $\Gamma_{ij}(\vec{x})$, is replaced by the projected Fisher matrix, $\gamma_{ij}(\vec{x})$. The projection of the k^{th} parameter is given by

$$\Gamma_{ij}^{n-1} = \Gamma_{ij}^n - \frac{\Gamma_{ik}^n \Gamma_{jk}^n}{\Gamma_{kk}^n}, \quad (29)$$

where n denotes the dimension of the projected matrix. Repeated application of the above projection yields $\gamma_{ij} = \Gamma_{ij}^{3N}$. Inverting γ_{ij} yields the same uncertainty estimates for the intrinsic parameters as one gets from the full Fisher matrix, but the covariances are much larger. The large covariances make it imperative that the proposal distributions use the eigenvalues and eigenvectors of γ_{ij} , as using the parameter directions themselves would lead to a slowly mixing chain.

V. F-STATISTIC MCMC

We implemented an F-statistic based MCMC algorithm using the approach described in §III, but with the full likelihood replaced by the F-statistic and the full Fisher matrix replaced by the projected Fisher matrix. Applying the F-MCMC search to the same data set as before yields the results summarized in Figure 2 and Table II. The recovered source parameters and signal-to-noise ratio (SNR = 10.4) are very similar to those found using the full 7-parameter search, but the F-MCMC estimates for the errors in the extrinsic parameters are very different. This is because the chain does not explore extrinsic parameters, but rather relies upon the F-statistic to find the extrinsic parameters that give the largest log likelihood based on the current values for the intrinsic

TABLE II: F-MCMC search for a single galactic binary

| | A (10^{-22}) | f (mHz) | θ | ϕ | ψ | ι | φ_0 |
|---------------------------------|--------------------|-----------|----------|--------|--------|---------|-------------|
| $\vec{\lambda}_{\text{True}}$ | 1.73 | 1.0005853 | 0.98 | 4.46 | 2.55 | 1.47 | 0.12 |
| $\vec{\lambda}_{\text{F-MCMC}}$ | 1.38 | 1.0005835 | 1.09 | 4.42 | 2.56 | 1.51 | 0.17 |
| σ_{Fisher} | 0.14 | 2.2e-06 | 0.089 | 0.052 | 0.055 | 0.051 | 0.22 |
| σ_{MCMC} | 0.02 | 2.5e-06 | 0.093 | 0.056 | 0.027 | 0.016 | 0.21 |

parameters. The effect is very pronounced in the histograms shown in Figure 2. Similar results were found for other F-MCMC runs on the same source, and for F-MCMC runs with other sources. Typical burn-in times were of order 1000 iterations, and the proposal acceptance rate was around 60%. As expected, the F-MCMC algorithm gave shorter burn-in times than the full parameter MCMC, and a comparable mixing rate.

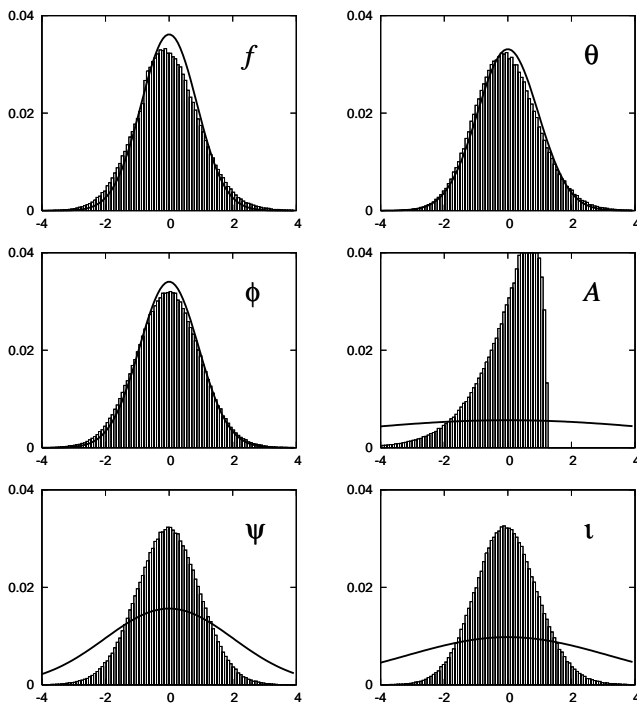


FIG. 2: Histograms showing the posterior distribution (grey) of the parameters. Also shown (black line) is the Gaussian approximation to the posterior distribution based on the Fisher information matrix. The mean values have been subtracted, and the parameters have been scaled by the square root of the variances calculated from the F-MCMC chains.

It is interesting to compare the computational cost of the F-MCMC search to a traditional F-Statistic based search on a uniformly spaced template grid. To cover the parameter space of one source (which for the current example extends over the full sky and 100 frequency bins) with a minimal match [34] of $\text{MM} = 0.9$ requires 39,000 templates [52]. A typical F-MCMC run uses less than 1000 templates to cover the same search space. The comparison becomes even more lopsided if we consider si-

multaneous searches for multiple sources. A grid based simultaneous search for two sources using the F-statistic would take $(39,000)^2 \simeq 1.5 \times 10^9$ templates, while the basic F-MCMC algorithm typically converges on the two sources in just 2000 steps. As the number of sources in the model increases the computation cost of the grid based search grows geometrically while the cost of the F-MCMC search grows linearly. It is hard to imagine a scenario (other than quantum computers) where non-iterative grid based searches could play a role in LISA data analysis.

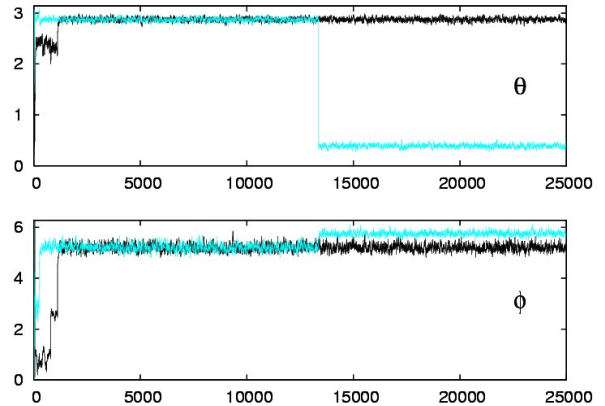


FIG. 3: Trace plots of the sky location parameters for two F-MCMC runs on the same data set. Both chains initially locked onto a secondary mode of the posterior, but one of the chains (light colored line) transitioned to the correct mode after 13,000 iterations.

While testing the F-MCMC algorithm on different sources we came across instances where the chain became stuck at secondary modes of the posterior. A good example occurred for a source with parameters $(A, f, \theta, \phi, \psi, \iota, \varphi_0) = (1.4\text{e-}22, 1.0020802\text{ mHz}, 0.399, 5.71, 1.3, 0.96, 1.0)$ and $\text{SNR} = 16.09$. Most MCMC runs returned good fits to the source parameters, with an average log likelihood of $\ln \mathcal{L} = 132$, mean intrinsic parameter values $(f, \theta, \phi) = (1.0020809\text{ mHz}, 0.391, 5.75)$ and $\text{SNR} = 16.26$. However, some runs locked into a secondary mode with average log likelihood $\ln \mathcal{L} = 100$, mean intrinsic parameter values $(f, \theta, \phi) = (1.0020858\text{ mHz}, 2.876, 5.20)$ and $\text{SNR} = 14.15$. It could sometimes take hundreds of thousands of iterations for the chain to discover the dominant mode. Figure 4 shows plots of the (inverted) likelihood \mathcal{L} and the log likelihood $\ln \mathcal{L}$ as a function of sky location for fixed $f = 1.0020802\text{ mHz}$. The log likelihood plot reveals the problematic secondary mode near the south pole, while the likelihood plot shows just how small a target the dominant mode presents to the F-MCMC search. Similar problems with secondary modes were encountered in the $f - \phi$ plane, where the chain would get stuck a full bin away from the correct frequency. These problems with the basic F-MCMC algorithm motivated

the embellishments described in the following section.

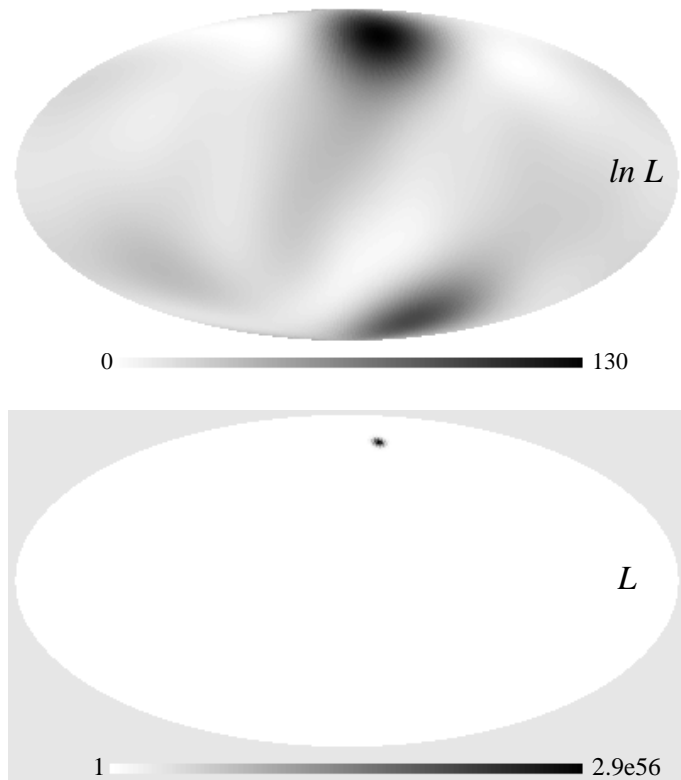


FIG. 4: Inverted likelihood and log likelihood as a function of sky location at fixed frequency.

VI. MULTIPLE PROPOSALS AND HEATING

The LISA data analysis problem belongs to a particularly challenging class of MCMC problems known as “mixture models.” As the name suggests, a mixture model contains a number of components, some or all of which may be of the same type. In our present study all the components are slowly evolving, circular binaries, and each component is described by the same set of seven parameters. There is nothing to stop two components in the search model from latching on to the same source, nor is there anything to stop one component in the search model from latching on to a blend of two overlapping sources. In the former instance the likelihood is little improved by using two components to model one source, so over time one of the components will tend to wander off in search of another source. In the latter instance it may prove impossible for any data analysis method to de-blend the sources (the marginal likelihood for the single component fit to the blended sources may exceed the marginal likelihood of the “correct” solution).

The difficulties we encountered with the single source searches getting stuck at secondary modes of the posterior are exacerbated in the multi-source case. Source overlaps can create additional secondary modes that are

not present in the non-overlapping case. We employed two techniques to speed burn-in and to reduce the chance of the chain getting stuck at a secondary mode: simulated annealing and multiple proposal distributions. Simulated annealing works by softening the likelihood function, making it easier for the chain to move between modes. The likelihood (8) can be thought of as a partition function $Z = C \exp(-\beta E)$ with the “energy” of the system given by $E = (s - h|s - h)$ and the “inverse temperature” equal to $\beta = 1/2$. Our goal is to find the template h that minimizes the energy of the system. Heating up the system by setting $\beta < 1/2$ allows the Markov Chain to rapidly explore the likelihood surface. We used a standard power law cooling schedule:

$$\beta = \begin{cases} \beta_0 \left(\frac{1}{2\beta_0} \right)^{t/T_c} & 0 < t < T_c \\ \frac{1}{2} & t \geq T_c \end{cases} \quad (30)$$

where t is the number of steps in the chain, T_c is the cooling time and β_0 is the initial inverse temperature. It took some trial and error to find good values of T_c and β_0 . If some of the sources have very high SNR it is a good idea to start at a high temperature $\beta_0 \sim 1/50$, but in most cases we found $\beta_0 = 1/10$ to be sufficient. The optimal choice for the cooling time depends on the number of sources and the initial temperature. We found that it was necessary to increase T_c roughly linearly with the the number of sources and the initial temperature. Setting $T_c = 10^5$ for a model with $N = 10$ sources and an initial temperature of $\beta_0 = 1/10$ gave fairly reliable results, but it is always a good idea to allow longer cooling times if the computational resources are available. The portion of the chain generated during the annealing phase has to be discarded as the cooling introduces an arrow of time which necessarily violates the reversibility requirement of a Markov Chain.

After cooling to $\beta = 1/2$ the chain can explore the likelihood surface for the purpose of extracting parameter estimates and error estimates. Finally, we can extract maximum likelihood estimates by “super cooling” the chain to some very low temperature (we used $\beta \sim 10^4$).

The second ingredient in our advanced F-MCMC algorithm is a large variety of proposal distributions. We used the following types of proposal distribution: $\text{Uniform}(\cdot, \vec{x}, i)$ - a uniform draw on all the parameters that describe source i , using the full parameter ranges, with all other sources held fixed; $\text{Normal}(\cdot, \vec{x})$ - a multivariate normal distribution with variance-covariance matrix given by $3N \times \gamma(\vec{x})$; $\text{Sky}(\cdot, \vec{x}, i)$ - a uniform draw on the sky location for source i ; $\sigma\text{-Uniform}(\cdot, \vec{x}, i)$ - a uniform draw on all the parameters that describe source i , using a parameter range given by some multiple of the standard deviations given by $\gamma(\vec{x})$. The $\text{Uniform}(\cdot, \vec{x}, i)$ and $\text{Normal}(\cdot, \vec{x})$ proposal distributions are the same as those used in the basic F-MCMC algorithm. The $\text{Sky}(\cdot, \vec{x}, i)$ proposal proved to be very useful at getting the chain away from secondary modes like the one seen in Figure 4, while the $\sigma\text{-Uniform}(\cdot, \vec{x}, i)$ proposal helped to move the

chain from secondary modes in the $f - \phi$ or $f - \theta$ planes. During the initial annealing phase the various proposal distributions were used in a cycle with one set of the bold distributions (Uniform, Sky and σ -Uniform) for every 10 draws from the timid multivariate normal distribution. During the main MCMC run at $\beta = 1/2$ the ratio of timid to bold proposals was increased by a factor of 10, and in the final super-cooling phase only the timid multivariate normal distribution was used.

The current algorithm is intended to give a proof of principle, and is certainly far from optimal. Our choice of proposal mixtures was based on a few hundred runs using several different mixtures. There is little doubt that a better algorithm could be constructed that uses a larger variety of proposal distributions in a more optimal mixture.

The improved F-MCMC algorithm was tested on a variety of simulated data sets that included up to 10 sources in a 100 bin snippet (once again we are using one year of observations). The algorithm performed very well, and was able to accurately recover all sources with $\text{SNR} > 5$ so long as the degree of source correlation was not too large. Generally the algorithm could de-blend sources that had correlation coefficients $C_{12} = (h_1|h_2)/\sqrt{(h_1|h_1)(h_2|h_2)}$ below 0.3. A full investigation of the de-blending of highly correlated sources is deferred to a subsequent study. For now we present one representative example from the 10 source searches.

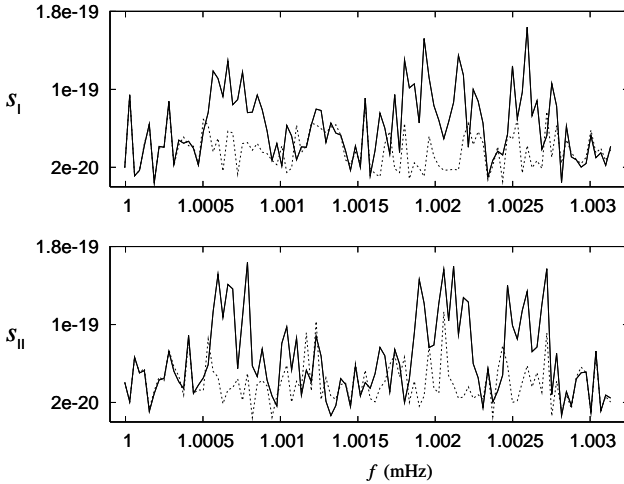


FIG. 5: Simulated LISA data with 10 galactic binaries. The solid lines show the total signal plus noise, while the dashed lines show the instrument noise contribution.

A set of 10 galactic sources was randomly selected from the frequency range $f \in [0.999995, 1.003164]$ mHz and their signals were processed through a model of the LISA instrument response. The root spectral densities in the two independent LISA data channels are shown in Figure 5, and the source parameters are listed in Table III. Note that one of the sources had a SNR below 5. The data was then search using our improved F-MCMC al-

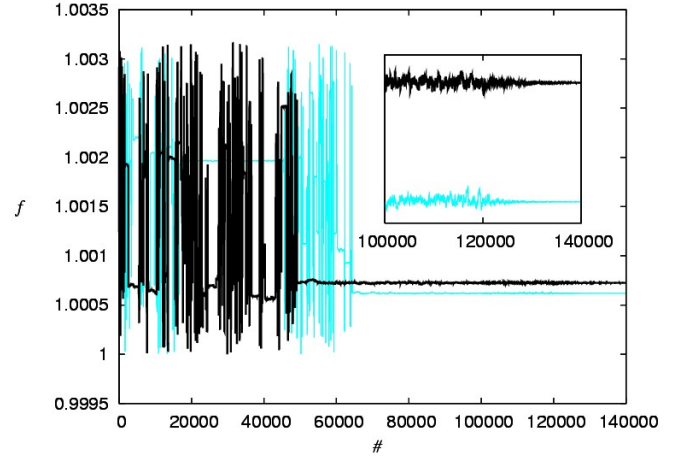


FIG. 6: Trace plots of the frequencies for two of the model sources. During the annealing phase ($\# < 10^5$) the chain explores large regions of parameter space. The inset shows a zoomed in view of the chain during the MCMC run at $\beta = 1/2$ and the final super cooling which starts at $\# = 1.2 \times 10^5$.

TABLE III: F-MCMC search for 10 galactic binaries using a model with 10 sources. The frequencies are quoted relative to 1 mHz as $f = 1 \text{ mHz} + \delta f$ with δf in μHz .

| | SNR | $A (10^{-22})$ | δf | θ | ϕ | ψ | ι | φ_0 |
|---------|------|----------------|------------|----------|--------|--------|---------|-------------|
| True | 8.1 | 0.56 | 0.623 | 1.18 | 4.15 | 2.24 | 2.31 | 1.45 |
| MCMC ML | 8.6 | 0.76 | 0.619 | 1.13 | 4.16 | 1.86 | 2.07 | 1.01 |
| True | 9.0 | 0.47 | 0.725 | 0.80 | 0.69 | 0.18 | 0.21 | 2.90 |
| MCMC ML | 11.3 | 0.97 | 0.725 | 0.67 | 0.70 | 0.82 | 0.99 | 1.41 |
| True | 5.1 | 0.46 | 0.907 | 2.35 | 0.86 | 0.01 | 2.09 | 2.15 |
| MCMC ML | 6.0 | 0.67 | 0.910 | 2.07 | 0.61 | 3.13 | 1.88 | 2.28 |
| True | 8.3 | 1.05 | 1.126 | 1.48 | 2.91 | 0.46 | 1.42 | 1.67 |
| MCMC ML | 6.9 | 0.75 | 1.114 | 1.24 | 3.01 | 0.40 | 1.26 | 2.88 |
| True | 8.2 | 0.54 | 1.732 | 1.45 | 0.82 | 1.58 | 0.79 | 2.05 |
| MCMC ML | 7.7 | 0.77 | 1.730 | 1.99 | 0.69 | 1.27 | 1.18 | 2.73 |
| True | 14.7 | 1.16 | 1.969 | 1.92 | 0.01 | 1.04 | 2.17 | 5.70 |
| MCMC ML | 12.8 | 1.20 | 1.964 | 1.97 | 6.16 | 0.97 | 2.00 | 6.15 |
| True | 4.9 | 0.41 | 2.057 | 2.19 | 1.12 | 1.04 | 2.13 | 3.95 |
| MCMC ML | 5.2 | 0.66 | 1.275 | 0.57 | 2.81 | 0.57 | 1.82 | 3.93 |
| True | 8.8 | 0.85 | 2.186 | 2.21 | 4.65 | 3.13 | 2.01 | 4.52 |
| MCMC ML | 10.0 | 1.01 | 2.182 | 2.43 | 5.06 | 0.26 | 2.00 | 5.54 |
| True | 7.6 | 0.58 | 2.530 | 2.57 | 0.01 | 0.06 | 0.86 | 0.50 |
| MCMC ML | 6.7 | 0.98 | 2.582 | 2.55 | 6.03 | 2.71 | 1.52 | 5.58 |
| True | 11.7 | 0.69 | 2.632 | 1.17 | 3.14 | 0.45 | 2.53 | 0.69 |
| MCMC ML | 13.5 | 1.39 | 2.627 | 1.55 | 3.07 | 3.08 | 1.94 | 6.07 |

gorithm using a model with 10 sources (70 parameters). The annealing time was set at 10^5 steps, and this was followed by a short MCMC run of 2×10^4 steps and a super cooling phase that lasted 2×10^4 steps. The main MCMC run was kept short as we were mostly interested in extracting maximum likelihood estimates. Figure 6 shows

a trace plot of the chain that focuses on the frequencies of two of the model sources. During the early hot phase the chain moves all over parameter space, but as the system cools to $\beta = 1/2$ the chain settles down and locks onto the sources. During the final super cooling phase the movement of the chain is exponentially damped as the model is trapped at a mode of shrinking width and increasing height.

The list of recovered sources can be found in Table III. The low SNR source (SNR = 4.9) was not recovered, but because the model was asked to find 10 sources it instead dug up a spurious source with SNR = 5.2. With two exceptions, the intrinsic parameters for the other 9 sources were recovered to within 3σ of the true parameters (using the Fisher matrix estimate of the parameter recovery errors). The two misses were the frequency of the source at $f = 1.00253$ mHz (out by 19σ) and the co-latitude of the source at $f = 1.002632$ mHz (out by 6σ). It is no coincidence that these misses occurred for the two most highly correlated sources ($C_{9,10} = -0.23$). The full source cross-correlation matrix is listed in (31).

$$C_{ij} = \frac{(h_i|h_j)}{\sqrt{(h_i|h_i)(h_j|h_j)}} = \begin{pmatrix} 1 & 0.08 & 0 & 0.01 & 0 & 0 & 0 & 0 & 0 & 0 \\ 0.08 & 1 & 0.02 & 0.01 & 0 & 0 & 0 & 0 & 0 & 0 \\ 0 & 0.02 & 1 & -0.06 & 0 & 0 & 0 & 0 & 0 & 0 \\ 0.01 & 0.01 & -0.06 & 1 & 0 & 0 & 0 & 0 & 0 & 0 \\ 0 & 0 & 0 & 0 & 1 & 0 & 0 & 0.01 & 0 & 0 \\ 0 & 0 & 0 & 0 & 0 & 1 & -0.03 & 0.03 & 0 & 0 \\ 0 & 0 & 0 & 0 & 0 & -0.03 & 1 & -0.05 & 0 & 0 \\ 0 & 0 & 0 & 0 & 0.01 & 0.03 & -0.05 & 1 & 0 & 0 \\ 0 & 0 & 0 & 0 & 0 & 0 & 0 & 0 & 1 & -0.23 \\ 0 & 0 & 0 & 0 & 0 & 0 & 0 & 0 & -0.23 & 1 \end{pmatrix} \quad (31)$$

The MCMC derived maximum likelihood estimates for the the source parameters can be used to regress the sources from the data streams. Figure 7 compares the residual signal to the instrument noise. The total residual power is below the instrument noise level as some of the noise has been incorporated into the recovered signals.

VII. MODEL SELECTION

In the preceding examples we used models that had the same number of components as there were sources in the data snippet. This luxury will not be available with the real LISA data. A realistic data analysis procedure will have to explore model space as well as parameter space. It is possible to generalize the MCMC approach to simultaneously explore both spaces by incorporating trans-dimensional moves in the proposal distributions. In other words, proposals that change the number of sources

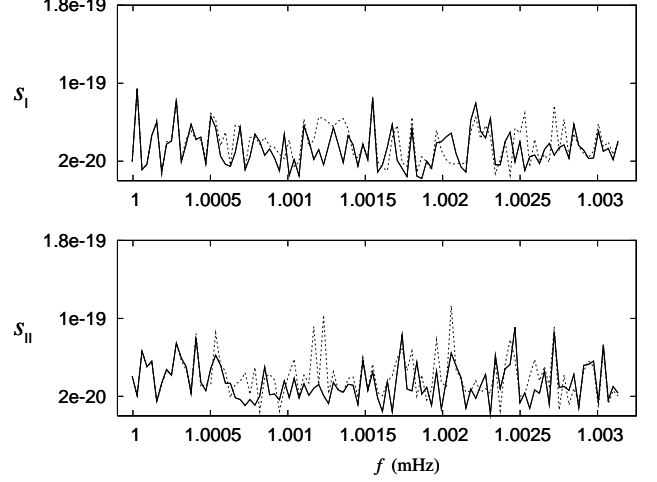


FIG. 7: The LISA data channels with the sources regressed using the maximum likelihood parameter estimates from the F-MCMC search. The solid lines show the residuals, while the dashed lines show the instrument noise contribution.

being used in the fit. One popular method for doing this is Reverse Jump MCMC [49], but there are other simpler methods that can be used. When trans-dimensional moves are built into the MCMC algorithm the odds ratio for the competing models is given by the fraction of the time that the chain spends exploring each model. While trans-dimensional searches provide an elegant solution to the model determination problem in principle, they can perform very poorly in practice as the chain is often reluctant to accept a trans-dimensional move.

A simpler alternative is to compare the outputs of MCMC runs using models of fixed dimension. The odds ratio can then be calculated using Bayes factors. Calculating the marginal likelihood of a model is generally very difficult as it involves an integral over all of parameter space:

$$p_X(s) = \int p(s|\vec{\lambda}, X) p(\vec{\lambda}, X) d\vec{\lambda}. \quad (32)$$

Unfortunately, this integrand is not weighted by the posterior distribution, so we cannot use the output of the MCMC algorithm to compute the integral. When the likelihood distribution has a single dominant mode, the integrand can be approximated using the Laplace approximation:

$$p(\vec{\lambda}, X) p(s|\vec{\lambda}, X) \simeq p(\vec{\lambda}_{\text{ML}}, X) p(s|\vec{\lambda}_{\text{ML}}, X) \times \exp\left(-\frac{(\vec{\lambda} - \vec{\lambda}_{\text{ML}}) \cdot F \cdot (\vec{\lambda} - \vec{\lambda}_{\text{ML}})}{2}\right). \quad (33)$$

where F is given by the Hessian

$$F_{ij} = \frac{\partial^2 \ln(p(\vec{\lambda}, X) p(s|\vec{\lambda}, X))}{\partial \lambda_i \partial \lambda_j} \Big|_{\vec{\lambda} = \vec{\lambda}_{\text{ML}}}. \quad (34)$$

TABLE IV: F-MCMC search for 10 galactic binaries using a model with 9 sources. The frequencies are quoted relative to 1 mHz as $f = 1 \text{ mHz} + \delta f$ with δf in μHz .

| | SNR | A (10^{-22}) | δf | θ | ϕ | ψ | ι | φ_0 |
|---------|------|--------------------|------------|----------|--------|--------|---------|-------------|
| True | 8.1 | 0.56 | 0.623 | 1.18 | 4.15 | 2.24 | 2.31 | 1.45 |
| MCMC ML | 8.6 | 0.77 | 0.619 | 1.12 | 4.16 | 1.86 | 2.06 | 1.02 |
| True | 9.0 | 0.47 | 0.725 | 0.80 | 0.69 | 0.18 | 0.21 | 2.90 |
| MCMC ML | 11.3 | 0.95 | 0.725 | 0.67 | 0.70 | 0.84 | 0.98 | 1.30 |
| True | 5.1 | 0.46 | 0.907 | 2.35 | 0.86 | 0.01 | 2.09 | 2.15 |
| MCMC ML | 6.2 | 0.75 | 0.910 | 2.09 | 0.61 | 3.09 | 1.82 | 2.21 |
| True | 8.3 | 1.05 | 1.126 | 1.48 | 2.91 | 0.46 | 1.42 | 1.67 |
| MCMC ML | 7.0 | 0.81 | 1.112 | 1.24 | 2.95 | 0.45 | 1.31 | 2.55 |
| True | 8.2 | 0.54 | 1.732 | 1.45 | 0.82 | 1.58 | 0.79 | 2.05 |
| MCMC ML | 7.5 | 0.76 | 1.730 | 1.95 | 0.70 | 1.23 | 1.19 | 2.68 |
| True | 14.7 | 1.16 | 1.969 | 1.92 | 0.01 | 1.04 | 2.17 | 5.70 |
| MCMC ML | 12.9 | 1.23 | 1.965 | 1.97 | 6.17 | 0.99 | 1.99 | 6.11 |
| True | 4.9 | 0.41 | 2.057 | 2.19 | 1.12 | 1.04 | 2.13 | 3.95 |
| MCMC ML | - | - | - | - | - | - | - | - |
| True | 8.8 | 0.85 | 2.186 | 2.21 | 4.65 | 3.13 | 2.01 | 4.52 |
| MCMC ML | 10.0 | 1.00 | 2.182 | 2.41 | 5.05 | 0.23 | 2.00 | 5.59 |
| True | 7.6 | 0.58 | 2.530 | 2.57 | 0.01 | 0.06 | 0.86 | 0.50 |
| MCMC ML | 5.8 | 0.72 | 2.536 | 0.58 | 5.70 | 3.04 | 1.52 | 4.64 |
| True | 11.7 | 0.69 | 2.632 | 1.17 | 3.14 | 0.45 | 2.53 | 0.69 |
| MCMC ML | 13.2 | 1.21 | 2.631 | 1.41 | 2.97 | 0.46 | 2.02 | 0.50 |

When the priors $p(\vec{\lambda}, X)$ are uniform or at least slowly varying at maximum likelihood, F_{ij} is equal to the Fisher matrix Γ_{ij} . The integral is now straightforward and yields

$$p_X(s) \simeq p(\vec{\lambda}_{\text{ML}}, X) p(s|\vec{\lambda}_{\text{ML}}, X) \frac{(2\pi)^{D/2}}{\det F}. \quad (35)$$

With uniform priors $p(\vec{\lambda}_{\text{ML}}, X) = 1/V$, where V is the volume of parameter space, and $(2\pi)^{D/2}/\det F = \Delta V$, where ΔV is the volume of the error ellipsoid.

To illustrate how the Bayes factor can be used in model selection, we repeated the F-MCMC search described in the previous section, but this time using a model with 9 sources. The results of a typical run are presented in Table IV. The parameters of the 9 brightest sources were all recovered to within 3σ of the input values, save for the sky location of the source with frequency $f = 1.00253$ mHz. It appears that confusion with the source at $f = 1.002632$ mHz may have caused the chain to favour a secondary mode like the one seen in Figure 4. Using (35) to estimate the marginal likelihoods for the 9 and 10 parameter models we found $\ln p_9(s) = -384.3$ and $\ln p_{10}(s) = -394.9$, which gives an odds ratio of $1 : 4 \times 10^4$ in favour of the 9 parameter model. In contrast, a naive comparison of log likelihoods, $\ln \mathcal{L}_9 = 413.1$ and $\ln \mathcal{L}_{10} = 425.7$ would have favoured the 10 parameter model.

It is also interesting to compare the output of the 10 source MCMC search to the maximum likelihood one gets

by starting at the true source parameters then applying the super cooling procedure (in other words, cheat by starting in the neighborhood of the true solution). We found $p_{\text{cheat}}(s) = -394.5$, and $\ln \mathcal{L}_{\text{cheat}} = 421.5$, which tells us that the MCMC solution, while getting two of the source parameters wrong, provides an equally good fit to the data. In other words, there is *no* data analysis algorithm that can fully deblend the two highly overlapping sources.

VIII. CONCLUSION

Our first pass at applying the MCMC method to LISA data analysis has shown the method to have considerable promise. The next step is to push the existing algorithm until it breaks. Simulations of the galactic background suggest that bright galactic sources reach a peak density of one source per five 1/year frequency bins [10]. We have shown that our current F-MCMC algorithm can handle a source density of one source per ten frequency bins across a one hundred bin snippet. We have yet to try larger numbers of sources as the current version of the algorithm employs the full $D = 7N$ dimensional Fisher matrix in many of the updates, which leads to a large computational overhead. We are in the process of modifying the algorithm so that sources are first grouped into blocks that have strong overlap. Each block is effectively independent of the others. This allows each block to be updated separately, while still taking care of any strongly correlated parameters that might impede mixing of the chain. We have already seen some evidence that high local source densities pose a challenge to the current algorithm. The lesson so far has been that adding new, specially tailored proposal distributions to the mix helps to keep the chain from sticking at secondary modes of the posterior (it takes a cocktail to solve the cocktail party problem). On the other hand, we have also seen evidence of strong multi-modality whereby the secondary modes have likelihoods within a few percent of the global maximum. In those cases the chain tends to jump back and forth between modes before being forced into a decision by the super-cooling process that follows the main MCMC run. Indeed, we may already be pushing the limits of what is possible using any data analysis method. For example, the 10 source search used a model with 70 parameters to fit 400 pieces of data (2 channels \times 2 Fourier components \times 100 bins). One of our goals is to better understand the theoretical limits of what can be achieved so that we know when to stop trying to improve the algorithm!

It would be interesting to compare the performance of the different methods that have been proposed to solve the LISA cocktail party problem. Do iterative methods like gCLEAN and Slice & Dice or global maximization methods like Maximum Entropy have different strengths and weakness compared to MCMC methods, or do they all fail in the same way as they approach the confusion

limit? It may well be that methods that perform better with idealized, stationary, Gaussian instrument noise will not prove to be the best when faced with real instrumental noise.

Acknowledgments

This work was supported by NASA Cooperative Agreement NCC5-579.

-
- [1] P. Bender *et al.*, *LISA Pre-Phase A Report*, (1998).
 - [2] C. R. Evans, I. Iben & L. Smarr, *ApJ* **323**, 129 (1987).
 - [3] V. M. Lipunov, K. A. Postnov & M. E. Prokhorov, *A&A* **176**, L1 (1987).
 - [4] D. Hils, P. L. Bender & R. F. Webbink, *ApJ* **360**, 75 (1990).
 - [5] D. Hils & P. L. Bender, *ApJ* **537**, 334 (2000).
 - [6] G. Nelemans, L. R. Yungelson & S. F. Portegies Zwart, *A&A* **375**, 890 (2001).
 - [7] L. Barack & C. Cutler, *Phys. Rev. D* **69**, 082005 (2004).
 - [8] J. R. Gair, L. Barack, T. Creighton, C. Cutler, S. L. Larson, E. S. Phinney & M. Vallisneri, *Class. Quant. Grav.* **21**, S1595 (2004).
 - [9] A. J. Farmer & E. S. Phinney, *Mon. Not. Roy. Astron. Soc.* **346**, 1197 (2003).
 - [10] S. Timpano, L. J. Rubbo & N. J. Cornish, *gr-qc/0504071* (2005).
 - [11] L. Barack & C. Cutler, *Phys. Rev. D* **70**, 122002 (2004).
 - [12] N. Metropolis, A. W. Rosenbluth, M. N. Rosenbluth, A. H. Teller & E. Teller, *J. Chem. Phys.* **21**, 1087 (1953).
 - [13] W. K. Hastings, *Biometrics* **57**, 97 (1970).
 - [14] N. Christensen & R. Meyer, *Phys. Rev. D* **58**, 082001 (1998); N. Christensen & R. Meyer, *Phys. Rev. D* **64**, 022001 (2001); N. Christensen, R. Meyer & A. Libson, *Class. Quant. Grav.* **21**, 317 (2004).
 - [15] N. Christensen, R. J. Dupuis, G. Woan & R. Meyer, *Phys. Rev. D* **70**, 022001 (2004); R. Umstätter, R. Meyer, R. J. Dupuis, J. Veitch, G. Woan & N. Christensen, *gr-qc/0404025* (2004).
 - [16] R. Umstätter, N. Christensen, M. Hendry, R. Meyer, V. Simha, J. Veitch, S. Viegand & G. Woan, *gr-qc/0503121* (2005).
 - [17] L. Page, S. Brin, R. Motwani & T. Winograd, *Stanford Digital Libraries Working Paper* (1998).
 - [18] M. Tinto, J. W. Armstrong & F. B. Estabrook, *Phys. Rev. D* **63**, 021101(R) (2001).
 - [19] C. Cutler, *Phys. Rev. D* **57**, 7089 (1998).
 - [20] N. J. Cornish & L. J. Rubbo, *Phys. Rev. D* **67**, 022001 (2003).
 - [21] T. A. Prince, M. Tinto, S. L. Larson & J. W. Armstrong, *Phys. Rev. D* **66**, 122002 (2002).
 - [22] C. W. Helstrom, *Statistical Theory of Signal Detection*, 2nd Edition (Pergamon Press, London, 1968).
 - [23] L. A. Wainstein and V. D. Zubakov, *Extraction of Signals from Noise* (Prentice-Hall, Englewood Cliffs, 1962).
 - [24] K. S. Thorne, in *300 Years of Gravitation*, edited by S. W. Hawking and W. Israel (Cambridge University Press, Cambridge, England, 1987), p. 330.
 - [25] B. F. Schutz, in *The Detection of Gravitational waves*, edited by D. G. Blair (Cambridge University Press, Cambridge, England, 1991), p. 406.
 - [26] B. S. Sathyaprakash and S. V. Dhurandhar, *Phys. Rev. D* **44**, 3819 (1991).
 - [27] S. V. Dhurandhar and B. S. Sathyaprakash, *Phys. Rev. D* **49**, 1707 (1994).
 - [28] C. Cutler and É. É. Flanagan, *Phys. Rev. D* **49**, 2658 (1994).
 - [29] R. Balasubramanian and S. V. Dhurandhar, *Phys. Rev. D* **50**, 6080 (1994).
 - [30] B. S. Sathyaprakash, *Phys. Rev. D* **50**, 7111 (1994).
 - [31] T. A. Apostolatos, *Phys. Rev. D* **52**, 605 (1996).
 - [32] E. Poisson and C. M. Will, *Phys. Rev. D* **52**, 848 (1995).
 - [33] R. Balasubramanian, B. S. Sathyaprakash, and S. V. Dhurandhar, *Phys. Rev. D* **53**, 3033 (1996).
 - [34] B. J. Owen, *Phys. Rev. D* **53**, 6749 (1996).
 - [35] B. J. Owen and B. S. Sathyaprakash, *Phys. Rev. D* **60**, 022002 (1999).
 - [36] L. S. Finn, *Phys. Rev. D* **46** 5236 (1992).
 - [37] P. Jaranowski & A. Krolak, *Phys. Rev. D* **49**, 1723 (1994).
 - [38] P. Jaranowski, A. Krolak & B. F. Schutz, *Phys. Rev. D* **58** 063001 (1998).
 - [39] M. H. A. Davis, in *Gravitational Wave Data Analysis*, edited by B. F. Schutz, (Kluwer Academic, Boston, 1989).
 - [40] F. Echeverria, *Phys. Rev. D* **40**, 3194 (1989).
 - [41] N. J. Cornish & S. L. Larson, *Phys. Rev. D* **67**, 103001 (2003).
 - [42] J. Högbom, *Astr. J. Suppl.* **15**, 417 (1974).
 - [43] N. J. Cornish, *Talk given at GR17, Dublin, July (2004)*; N. J. Cornish, L. J. Rubbo & R. Hellings, *in preparation* (2005).
 - [44] G. Schwarz, *Ann. Stats.* **5**, 461 (1978).
 - [45] *Markov Chain Monte Carlo in Practice*, Eds. W. R. Gilks, S. Richardson & D. J. Spiegelhalter, (Chapman & Hall, London, 1996).
 - [46] D. Gamerman, *Markov Chain Monte Carlo: Stochastic Simulation of Bayesian Inference*, (Chapman & Hall, London, 1997).
 - [47] C. Andrieu, N. De Freitas, A. Doucet & M. Jordan, *Machine Learning* **50**, 5 (2003).
 - [48] L. Tierney & A. Mira, *Statistics in Medicine* **18**, 2507 (1999).
 - [49] P. J. Green & A. Mira, *Biometrika* **88**, 1035 (2001).
 - [50] L. J. Rubbo, N. J. Cornish & O. Poujade, *Phys. Rev. D* **69** 082003 (2004).
 - [51] A. Krolak, M. Tinto & M. Vallisneri, *Phys. Rev. D* **70**

022003 (2004).

[52] N.J. Cornish & E.K. Porter, gr-qc/0504012 (2005).